Full Paper

Propellants, Explosives, Pyrotechnics

DOI: 10.1002/prep.201400184

The Effect of Pore Morphology on Hot Spot Temperature

George Arthur Levesque*[a] and Peter Vitello[b]

Abstract: Composite explosives contain pores that collapse under shock wave interaction generating localized regions of heat known to be important in the initiation of high explosives. Understanding pore collapse under shock loading is essential to create predictive reactive flow models to simulate the initiation process. While spherical pore collapse has been thoroughly simulated, other geometries have been relatively neglected. Simulating microoscale hot spot nucleation, we analyze the effect of pore morphology on the post-shock hot spot temperature. Several pore morphologies that yield higher temperatures than the spherical case are revealed and discussed. This work performed under the auspices of the U.S. Department of Energy by Lawrence Livermore National Laboratory under Contract DE-AC52-07NA27344.

Keywords: Pore collapse · Microscale simulation · Explosive initiation · Pore shape

1 Introduction

Insensitive explosives are intentionally initiated by transmitting a shock wave. This shock wave heats the explosive composite, but not enough for thermal decomposition on its own. The mechanism of initiation is attributed to localized heating sites (referred to as hot spots), to which there are many attributed mechanisms including: (a) hydrodynamic pore collapse [1], (b) shear [2], (c) viscoplastic material heating [3], (d) work on trapped gases [4], (e) mach stems and more [5]. Thermal energy calculations suggested that collapsing pores are the most effective mechanism [6]. In addition, experiment has shown that composites with more porosity are more sensitive to shock initiation [7]. As a result, hot spot nucleation has been mainly attributed to pore collapse.

Analysis on pore collapse is not hard to find [8,9]. For small pores in materials of high viscosity, there are simplified axisymmetric partial differential equations to analyze the amount of heat generated post-collapse [3,6,10,11]. There are computational analyses in continuum hydrodynamics of pore collapse on the microscale of varying resolution and complexity [12] and in molecular dynamics simulations of pore collapse (which are limited by domain size) [13–16]. There are also analyses of fields of pores to examine interaction during collapse [17] and ambitious microscale simulations for the run-to-detonation evolution [18]. Despite all this analysis, the only articles to explore a non-spherical pore collapse is in Ref. [19], where a sphere and a triangle are analyzed and more recently, perturbed shapes have been investigated in Ref. [20].

While a sphere might be the average of all pore shapes about their centroids, pores are not commonly spherical. In an explosive crystal, a pore could be of any geometry of missing molecules in a lattice. In the synthesis of explosive composites, rough explosive crystal grains are coated with plasticized binder materials forming prills. These prills are pressed under high pressure and vacuum to generate a high density part. Even if a prill formed with a spherical bubble, it is unlikely to remain spherical in the pressing process [21]. Additionally, even if the average shape was spherical, this does not necessarily mean that the average shape will generate an average amount of thermal energy when compared to the full range of pore shapes. Researchers have still gravitated to the spherical pore for the bulk of their analyses. Herein, differences in thermal energy as a function of pore morphology are analyzed and discussed.

2 Analysis

In prior work, we have simulated pore collapse using a highly-parallelized arbitrary-Lagrangian/Eulerian multiphysics hydrocode, ALE3D, in combination with the thermochemical code, CHEETAH, which supplies equation of state information at every time step to the multiphysics hydrocode [12,22,23]. Herein, we simulate the collapse behavior

[a] *G. A. Levesque*
Physical and Life Sciences
Lawrence Livermore National Laboratory
7000 East Avenue,L-288
Livermore, CA 94550, USA
**e-mail: Levesque6@llnl.gov*

[b] *P. Vitello*
Physical and Life Sciences
Lawrence Livermore National Laboratory
7000 East Avenue,L-170
Livermore, CA 94550, USA

of axisymmetric pores, with nanometer-scale refinement, of differing morphologies but identical volumes. All pores are subjected to shock pressures, P_s, of 10 GPa in triaminotrinitrobenzene (TATB) material, which is simulated as having a constant viscosity of 4.6 Pa·s [24]. While chemical kinetics for TATB decomposition are available, [25] the explosive is treated as inert to understand the effect of pore morphology on the unreacted material.

The 2D cylindrical model consists of a continuum TATB material and an air-filled void, where both are initially set to ambient temperature (293 K) and pressure (101.3 kPa). The boundary conditions of the 2D rectangular space are symmetry boundary conditions in the *y* direction constraining the top and bottom, an axis of symmetry horizontally through the pore's equator, a velocity loading on the left boundary (which initiates the shock that propagates to the right across our analyzed pore), and a non-reflective outflow boundary on the right (see Figure 1). Sensitivity studies direct simulations to have 80,000 elements and run for about 120 h on 8 processors. Analysis of pore closure was done for a variety of pore shapes (ellipses, cones, and cylinders) under the passing shockwave.

2.1 Spherical Pore

In Ref. [12], we analyzed spherical pores of various radii interacting with several shock pressures. Herein we investigate pores of different shapes. We have constrained simulations of all pores to the same volume of a 1 μm radius spherical pore. This will isolate the range of the effect of morphology alone for a material with a constrained porosity. The pore collapse evolution of the 1 μm radius spherical pore is illustrated in Figure 2 (legend for temperature plots, see Figure 3).

The visualization of pore collapse temperature fields are useful to understand the collapse evolution but it is a challenge to understand exactly which hot spots generate the most heat relative to each other. This is especially true for simulations with axisymmetry as areas away from the axis can have much more mass at a given temperature than those areas close to that axis. To elucidate, histograms of temperature are gathered for each collapsed pore to compare temperature fields for each generated hot spot. The data for these plots is from a time after the total thermal energy is at a maximum which is always after pore collapse is complete. For subsequent analyses of this type, the time that data is extracted is different for each pore shape since they require different times to collapse. For the spherical pore, the data of the post-collapse temperature field is plotted in Figure 4. The *y* axis of this plot shows the amount of mass (in picograms) per radian of revolution

Figure 2. Temperature plots of an evolving pore collapse at times $t = -1.0$, 0.7, 1.3, 2.1, and 2.5 ns (where $t = 0$ is when the shock reaches the pore). The temperature scale is seen in Figure 3.

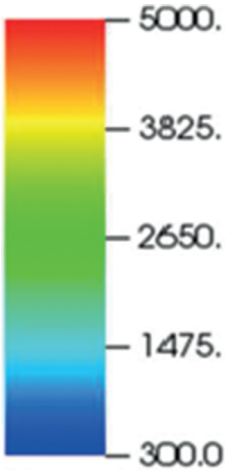

Figure 3. A legend for the temperature plots in degrees Kelvin as in Figure 2 above and all such figures to come.

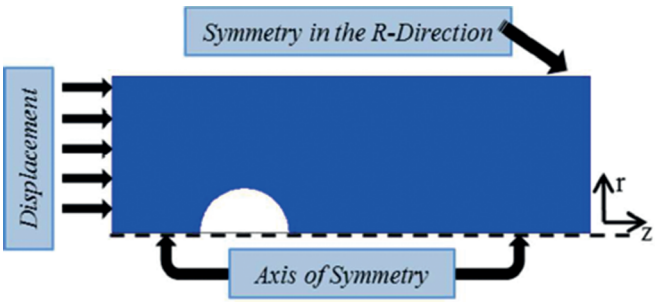

Figure 1. Illustration of the simulation space and the boundary conditions.

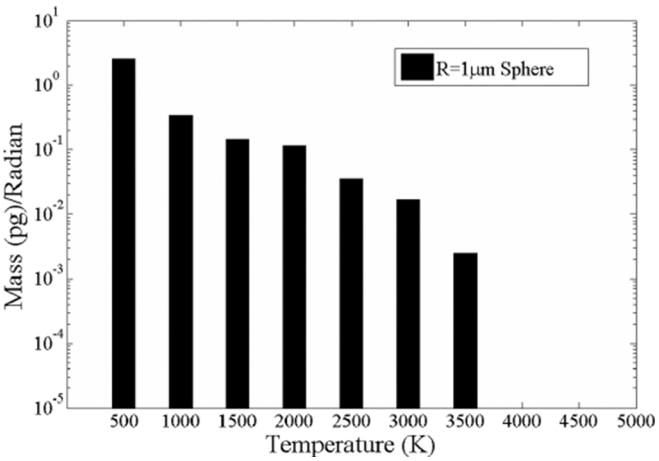

Figure 4. Histogram of temperature resulting from the collapse of a spherical pore.

about the axis of symmetry and is plotted on a log-scale to display the small masses at high temperatures that would react instantly in the presence of active chemistry.

2.2 Elliptical Pores

Elliptical pores were examined under collapse to determine the effect of perturbations on the spherical geometry on hot spot temperature. Since these pores had the same volume as a 1 μm radius pore, and it was simulated in 2D on the axis of symmetry, than the dimensions of the ellipsoid were constrained by the relationship in Equation (1).

$$a = \frac{1}{b^2} \tag{1}$$

Here a is the semi-principal axis on the axis of symmetry and b is the semi-principal axis in the radial dimension. Oblate elliptical pores of dimension $b = 1.25$, 1.5, and 1.75 μm were subjected to the analysis, as well as prolate ellipsoids of dimension $a = 1.25$, 1.5, and 1.75 μm. The evolution of the temperature fields are plotted in Figure 5 and Figure 6. The histograms of mass at different temperatures are presented in Figure 7 and Figure 8.

A few trends are important to note. Firstly, all prolate ellipsoids that have $a > 1$ have more mass at higher temperatures than the spherical case (where $a = 1$). Secondly, all oblate ellipsoids, with $a < 1$, had less mass at higher tem-

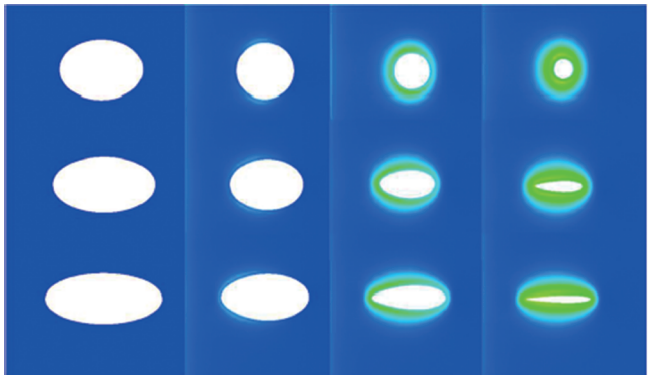

Figure 5. Evolving elliptical pore collapses of dimensions $a = 1.25$, 1.50, and 1.75 μm. Images are shown for time $t = -1$, 1, 2, and 3 ns.

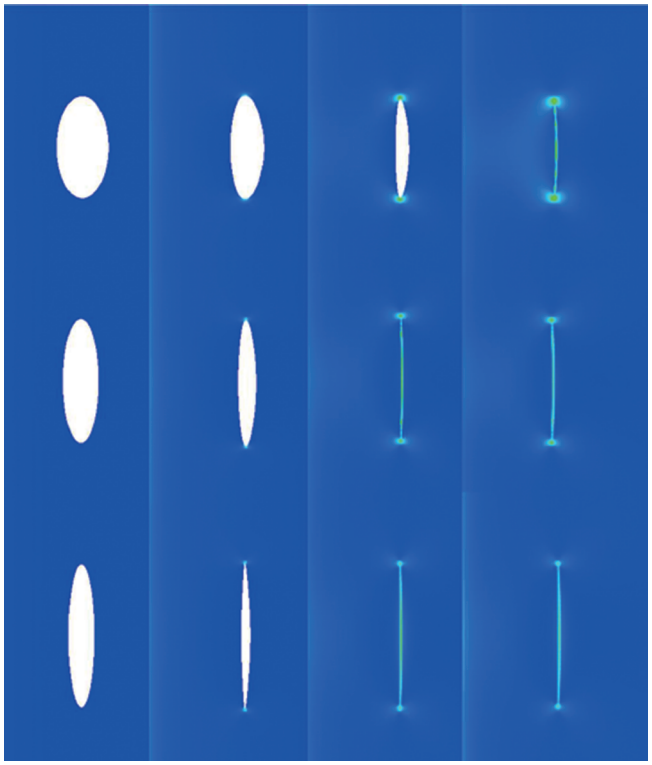

Figure 6. Evolving elliptical pore collapses of dimensions $b = 1.25$, 1.50, and 1.75 μm. Images are shown for times $t = -0.2$, 0.3, 0.7, and 1.05 ns.

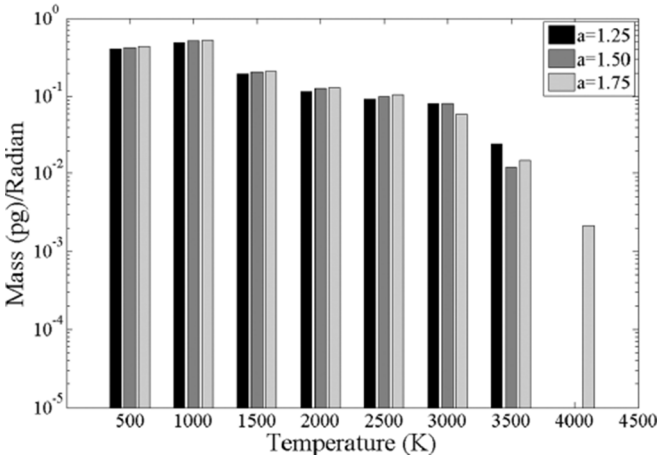

Figure 7. Histogram of temperature resulting from the collapse of oblate ellipsoidal pores of dimension $a = 1.25$, 1.50, and 1.75 μm.

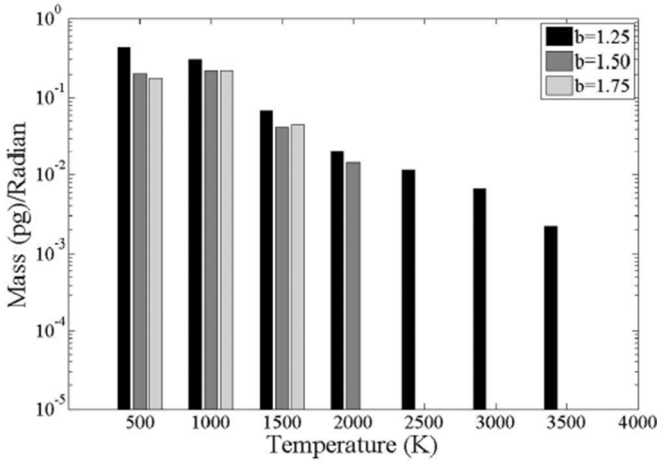

Figure 8. Histogram of temperature resulting from the collapse of prolate ellipsoidal pores of dimension $b = 1.25$, 1.5, and 1.75 μm.

peratures than the spherical case, despite having identical volumes. The results indicate that pores that are longer in the direction of shock propagation had developed significantly more thermal energy than those who had their shortest axis on the symmetry plane.

2.3 Cylindrical Pores

By introducing a rectangle on the axis of symmetry, we generate cylindrical pores. Since we are constraining the volume to be equal to the spherical pore, the relative dimensions are constrained by Equation (2).

$$h = \frac{4}{(3 * r^2)} \tag{2}$$

We have conducted simulations for cylindrical pores of dimension $r = 1.00$, 0.75, and 0.50 μm. Evolutions of the temperature fields of each are displayed in Figure 9. Histograms are again provided in Figure 10.

Again, we witness the trend that the elongated shapes in the direction of shock travel can create hotter hot spots. This brings into question what the limitations are in simulating with a constant viscosity. If we simulated an indefinitely long pore, our temperatures would be high as the relative shear would also increase in the absence of strength mechanisms that would break-up the shearing medium. An in situ measurement of average temperature of post-collapsed hot spots of different elongations would be a challenging but a relevant test to the limitations of our treatments of strength.

2.4 Conical Pores

Conical pores seem quite unlikely to occur in nature but it is a simple shape that allows us to examine the effect of sharp edges. Additionally, hollow and shaped charges, which rely on conical cavities in their design, have demonstrated the profound impact of the Monroe effect on macroscale explosive performance. Maybe if such a pore shape existed its ability to focus material in dynamic conditions could translate into making more effective hot spots.

By shaping a triangle onto the axis of revolution, we simulate cone-shaped pores. With one apex on the axis of symmetry and we must choose whether this points towards the oncoming shockwave or in the direction of shock travel. In addition to the choice of orientation, the height and width of the pore must be chosen. Since the volume is constrained to that of a 1 μm spherical pore, the relation in Equation (3) constrains the relative dimensions of the pore. We investigated three aspect ratios of cone height, h, to base radius, r, ($r/h = 0.33$, 0.5, and 1) in two orientations each.

$$r = \frac{2}{\sqrt{h}} \tag{3}$$

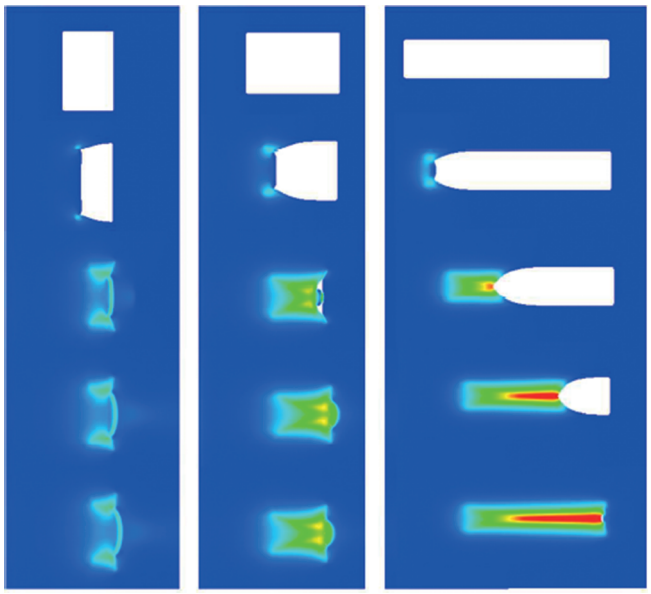

Figure 9. Cylindrical pores of different radii (from left to right, $r =$ 1.0, 0.75, and 0.5 μm) at (from top to bottom) $t = 0$, 0.35, 0.70, 1.05, 1.4 ns.

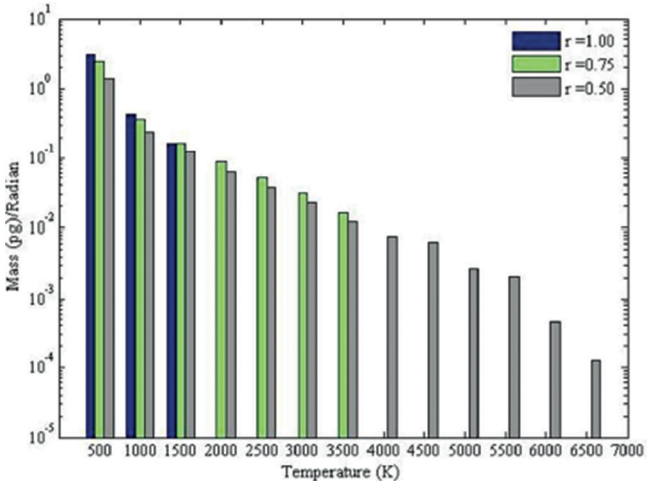

Figure 10. Histogram of mass vs. temperature for cylindrical pores of different aspect ratios.

Evolutions of the temperature field are seen in Figure 11 and Figure 12. There are two clear trends in these figures. Cones that have a longer aspect ratio generate more heat. Additionally, conical pores whose apex is pointing away from the oncoming shock generate much more heat. This is supported by the histograms in Figure 13 and Figure 14. This is the opposite direction of the designs in hollow and shaped charges. The difference here is that the emphasis in hollow/shape charges is to focus a converging jet of material for maximum velocity and, if possible, maximum heating would be avoided in the evolving jet to preserve strength. Another important difference is the length-scale

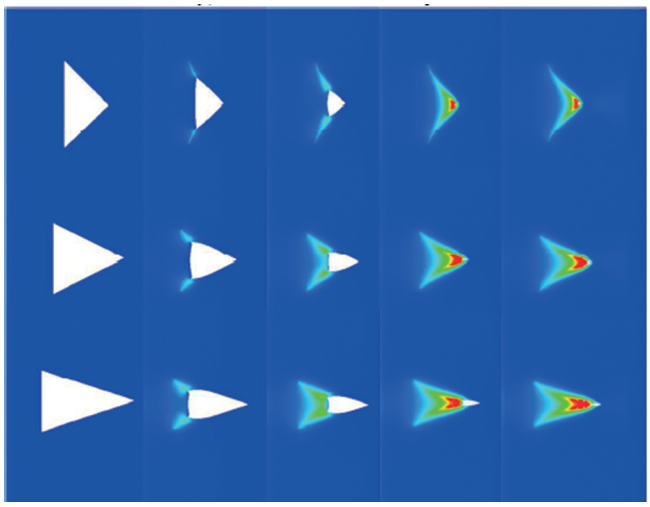

Figure 11. Three conical pores (with dimensions $r/h = 1$, 0.5, and 0.33 from top to bottom) with a point on the far end of shock travel. At times $t = -0.15$, 0.15, 0.3, 0.45, and 0.6 ns.

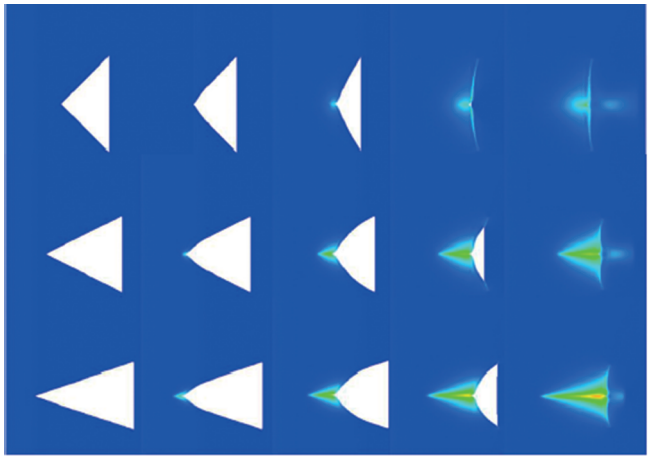

Figure 12. Three conical pores (with dimensions $r/h = 1$, 0.5, and 0.33 from top to bottom) with a point on the near end of shock travel. At times $t = -0.25$, 0, 0.25, 0.5, 0.75 ns.

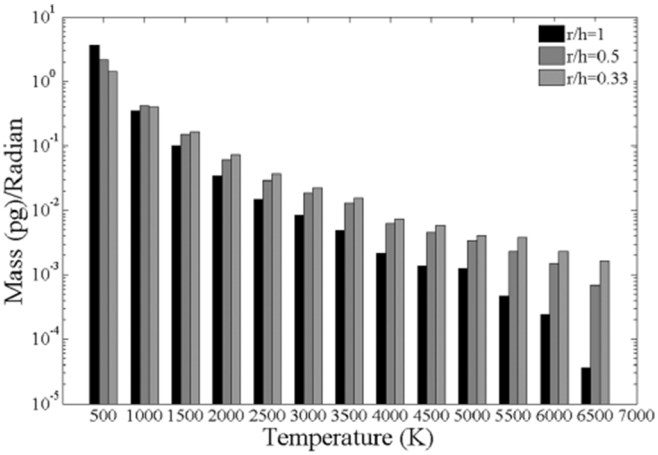

Figure 13. Histogram of mass vs. temperature for conical pores whose flat side is closer to the approaching shock than its tip, as seen in Figure 11.

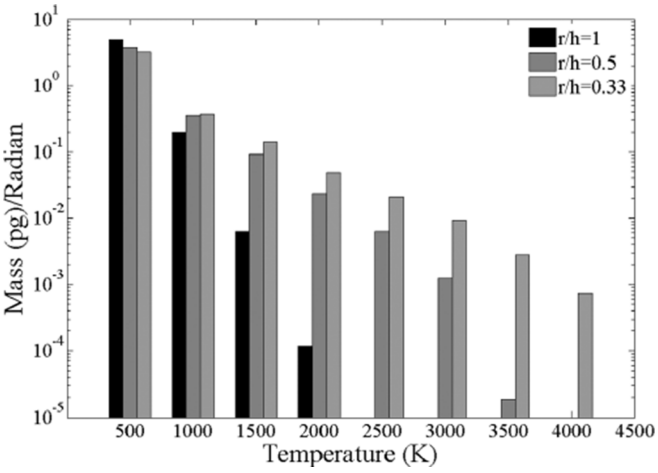

Figure 14. Histogram of mass vs. temperature for conical pores whose tip is closer to the approaching shock than its base as seen in Figure 12.

of the conical pore. Conical voids in hollow/shaped charges are on the cm scale and we are simulating on the μm-nm scale. The effect of the significantly smaller scale is that a convergent jet is difficult to achieve as a result of the strength that remains. Here, a jet is not traversing across our pore, but if we increased the size of these voids (or decreased viscosity) we should create a jet.

3 Conclusions

Continuum hydrodynamic simulations on the microscale were done to examine the effect of pore morphology on post-shock hot spot temperature distributions. A 1 μm radius spherical pore was simulated as a baseline for comparison. Then elliptical, conical, and cylindrical pores of the same volume were simulated and their temperature fields characterized.

Reflecting on the temperature distributions, elliptical pores generated more mass at high temperatures (above 3500 K) when their longest dimension was in line with the direction of shock travel. In fact as this dimension decreases, so does the amount of mass at high temperature. If their longest dimension was perpendicular to shock travel, there was less high temperature material than the spherical case.

Cylindrical pores (Section 2.3) also saw increasing temperatures as the on-axis dimension increased. Long cylinders allowed much viscous flow of the high explosive material (treated as a fluid). The treatment of material strength at high-strain rate on these small scales must be probed

further in the hope of making more predictive analysis of the temperature field that results from pore collapse.

Performance of the conical voids was best when the apex was farthest from the approaching shock; this is in the opposite orientation of macroscopic hollow or shaped charges. Conversely, if the pore pointed toward the oncoming shockwave, it usually generated less heat than the spherical pore but, as seen with other geometries, as the length of the cone increased on-axis, temperatures increased. A conical pore generated the most mass at high temperatures of the morphologies examined.

Historically, spherical pores have been the most analyzed; either for their relatively simple shape or because they are the average shape about the centroid of a wide-distribution of shapes and orientations. In our analysis, they do not generate the most, or seemingly even an average, amount of heat. Future studies are encouraged to acknowledge the spherical pore as a simplification and a rigorous analysis should consider a wide-variety of existing pore morphologies.

Acknowledgments

This work performed under the auspices of the U.S. Department of Energy by Lawrence Livermore National Laboratory under Contract DE-AC52-07NA27344.

References

[1] C. L. Mader, J. D. Kershner, *The Three-Dimensional Hot Spot Model Applied to PETN, HMX, TATB and NQ*, Los Alamos National Laboratory, LA-10203-MX UC-45, Los Alamos, NM, USA, **1984**.

[2] R. B. Frey, The Initiation of Explosive Charges by Rapid Shear, *7th International Detonation Symposium*, Annapolis, MD, USA, 16–19 June, **1981**, pp. 36–42.

[3] B. Khasainov, A. Attetkov, A. Borisov, Shock-Wave Initiation of Porous Energetic Materials and Viscous-Plastic Model of Hot Spot, *Khimicheskaya Fizika* **1996**, *15*, 53 – 125.

[4] Y. Partom, A Void Collapse Model for Shock Initiation, *7th International Detonation Symposium*, Annapolis, MD, USA, 16–19 June, **1981**, pp. 506–516.

[5] J. Field, N. Bourne, S. Palmer, S. Walley, J. Smallwood, Hot-Spot Ignition Mechanisms For Explosives And Propellants, *Phil. Trans. R. Soc. A* **1992**, *339*, 269 – 283.

[6] R. B. Frey, Cavity Collapse in Energetic Materials, *8th International Detonation Symposium*, Albuquerque, NM, USA, 15–19 June, **1985**, pp. 68–80.

[7] R. L. Gustavsen, S. A. Sheffield, R. R. Alcon, L. G. Hill, R. E. Winter, D. A. Salisbury, P. Taylor, Initiation of EDC-37 Measured with Embedded Electromagnetic Particle Velocity Gauges, *Shock Compression Condens. Matter* **1999**, 879–882.

[8] N. Bourne, J. Field, Shock-Induced Collapse of Single Cavities in Liquids, *J. Fluid Mech.* **1992**, *244*, 225 – 240.

[9] L. E. Fried, F. Najjar, W. M. Howard, M. R. Manaa, E. J. Reed, N. Goldman, S. Bastea, A. L. Nichols III, Multiscale Simulation of Hot Spot Ignition, *14th International Detonation Symposium,* Coeur d'Alene, ID, USA, 11–16 April, **2010**, pp. 1412–1421.

[10] D. E. Maiden, *A Model for Calculating the Threshold for Shock Initiation of Pyrotechnics and Explosives*, No. UCRL-96360, Lawrence Livermore National Laboratory, Livermore, CA, USA, **1987**.

[11] M. Carroll, A. Holt, Static and Dynamic Pore-Collapse Relations for Ductile Porous Materials, *J. Appl. Phys.* **1972**, *43*, 1626 – 1636.

[12] G. Levesque, P. Vitello, W. Howard, Hot-spot Contributions in Shocked High Explosives from Mesoscale Ignition Models, *J. Appl. Phys.* **2013**, *113*, 233513 – 233522.

[13] R. Shan, Atomistic Simulation of Nanoscale Void-Enhanced Initiation in Hexanitrostilbene, *15th International Detonation Symposium*, San Francisco, CA, USA, 13–16 July, **2014**.

[14] T.-R. Shan, A. P. Thompson, Micron-scale Reactive Atomistic Simulations of Void Collapse and Hotspot Growth in Pentaerythritol Tetranitrate, *15th International Detonation Symposium*, San Francisco, CA, USA, 13–16 July, **2014**.

[15] R. Shan, R. R. Wixom, A. P. Thompson, Nanoscale Void-enhanced Initiation in Hexanitrostilbene, *15th International Detonation Symposium*, San Francisco, CA, USA, 13–16 July, **2014**.

[16] T.-R. Shan, A. P. Thompson, Shock-Induced Hotspot Formation and Chemical Reaction Initiation in PETN Containing a Spherical Void, *18th APS-SCCM and 24th AIRAPT*, Seattle, WA, USA, 7–12 July, **2013**.

[17] A. Kapahi, H. S. Udaykumar, Dynamics of Void Collapse in Shocked Energetic Materials: Physics of Void-void Interactions, *Shock Waves* **2013**, *23*, 537–558.

[18] H. K. Springer, C. M. Tarver, J. E. Reaugh, C. M. May, Investigating Short-Pulse Shock Initiation in HMX-Based Explosives With Reactive Meso-Scale Simulations, *J. Phys.: Conf. Ser.* **2013**, 6.

[19] L. Tran, H. S. Udaykumar, Simulations of Void Collapse in an Energetic Material, Part 1: Inert Case, *J. Propul. Power* **2006**, *22*, 947–958.

[20] D. Damm, Development of a Grain-Scale Model for Initiation of HNS, *15th International Detonation Symposium*, San Francisco, CA, USA, 13–16 July, **2014**.

[21] T. M. Willey, L. Lauderbach, F. Gagliardi, B. Cunningham, K. T. Lorenz, J. Lee, T. van Buuren, R. Call, L. Landt, G. Overturf, Comprehensive Characterization of Voids and Microstructure in TATB-based Explosives from 10 nm to 1 cm: Effects of Temperature Cycling and Compressive Creep, *10th International Detonation Symposium*, Coeur de Alene, ID, USA, 11–16 April, **2010**, pp. 530–538.

[22] F. Najjar, W. Howard, L. Fried, M. Manaa, A. Nichols, G. Levesque, M. Elert, W. Buttler, J. Borg, J. Jordan, T. Vogler, Computational Study of 3-D Hot-Spot Initiation in Shocked Insensitive High-Explosive, *Shock Compress. Condens. Matter* **2012**, *1426*, 255–258.

[23] S. Bastea, L. E. Fried, Chemical Equilibrium Detonation, in: *Shock Wave Science and Technology Reference Library*, (Ed.: F. Zhang) Springer, Heidelberg, **2012**, pp. 1.

[24] L. Fried, L. Zepeda-Ruis, W. Howard, F. Najjar, J. Reaugh, M. Elert, W. Buttler, J. Borg, J. Jordan, T. Vogler, The Role of Viscosity in TATB Hot Spot Ignition, *Shock Compress. Condens. Matter* **2012**, *1426*, 299–302.

[25] M. Manaa, E. Reed, L. Fried, N. Goldman, Nitrogen-rich *Heterocycles* as Reactivity Retardants in Shocked Insensitive Explosives, *J. Am. Chem. Soc.* **2009**, *131*, 5483–5487.

Received: August 2, 2014
Revised: October 10, 2014
Published online: November 21, 2014

